Vol. 1 No. 2 JOURNAL OF COMPUTATIONAL MATHEMATICS April 1983

FOURTEEN-NODE MIXED STIFFNESS ELEMENT AND ITS COMPUTATIONAL COMPARISONS WITH TWENTY-NODE ISOPARAMETRIC ELEMENT

ZHOU TIAN-XIAO(周天孝), LI SHOU-LI(李守礼),
WANG ZHENG-WEI(王徵伟), XING JIAN-MIN(邢建民), YANG PING(阳 平)
(Computing Institute, Chinese Aeronautical Establishment)

Abstract

In this paper, a family of 3-dimensional elements different from isoparametric serendipity is developed according to the variational principle and the convergence criteria of the mixed stiffness finite element method[8,9,10]. For the new family, which is named mixed stiffness elements, the number of nodes on the quadratic (resp. cubic) element is not 20 (resp. 32) but 14 (resp. 26). Theoretical analysis and various computational comparisons have found the mixed stiffness element superior over the isoparametric serendipity element, especially a substantial improvement in computational efficiency can be achieved by replacing the 20 node-isoparametric element with the 14-node mixed stiffness element.

1. Introduction

For finite element analysis of a 3-dimensional continuum, an extensively used quadratic element is the 20-node isoparametric element. The element with the serendipity family as shape functions is sophisticated and has many advantages, but its practical use in large-scale problems always leads to very high requirement for computer memory capacity and to large amount of computational work.

The trouble is caused by excesive nodes over one element. Hence a question: Can another kind of distorted rectangular block elements with less than 20 nodes and the same accuracy be constructed? The history of the finite element method has indicated that it seems impossible to find any such element in the domain of standard finite elements. Recent advances of nonstandard finite element methods[1-3,5-9] make it possible to take another way and consequently give an affirmative answer to the question. By means of the mixed stiffness finite element method[8-10], a new family of curved elements is developed in the paper. A progressively increasing number of nodes and hence improved accuracy characterize each new member of the family. With the exception of the linear element, the number of nodes on each element of the new family is less than that of old serendipity family by six. For quadratic and cubic elements, they are 14 and 26 respectively.

Despite of the frequent use of linear and cubic elements in engineering design offices, we will focus our discussion, on account of the typicalness and practical importance of the quadratic element, on the 14-node mixed stiffness element. Through theoretical analysis and computational comparison with the 20-node isoparametric element, we will see that the performance of the new elements is quite satisfactory.

The paper is outlined as follows. In Sect. 2 the variational formulations of the

mixed stiffness method are briefly introduced. Sect. 3 is devoted to description of the essentials of direct formulation. In Sect. 4 three convergence criteria of the mixed stiffness method are posed, and the approximation of the 14-node element examined. Sect. 5 is concerned with computational comparisons. Sect. 6 is the conclusion.

2. Mixed Stiffness Finite Element Method

Let us consider the basic boundary problem of elasticity

$$-B^T\left(\frac{\partial}{\partial x_i}\right)DB\left(\frac{\partial}{\partial x_i}\right)\tilde{u}=f, \text{ in } \Omega, \tag{2.1}$$

$$\tilde{u}\,|_{\Gamma_u}=u_0, \tag{2.2}$$

$$T(\tilde{u})\,|_{\Gamma_\sigma}=T_0, \tag{2.3}$$

where $B\left(\frac{\partial}{\partial x_i}\right)$ = matrix of differential operator defining the strain-displacement relations,

D = elastic matrix,

T = vector of surface tractions and $T(u)=B^T(\cos(n, x_i))\,DB\left(\frac{\partial}{\partial x_i}\right)u$, where n is the surface normal,

Γ_σ = boundary of the domain Ω over which tractions T_0 are prescribed,

Γ_u = boundary of Ω over which displacements u_0 are prescribed, and $\Gamma_u=\partial\Omega\backslash\Gamma_\sigma$,

f = distributed body force.

A variational formulation equivalent to the boundary-value problem can be expressed as[8, 9]

$$\begin{aligned}\Pi_R^*=-\sum_n\Big\{&\int_{\Omega_n^*}\Big[\frac{1}{2}\,\sigma^TD^{-1}\sigma+f\cdot u\Big]d\Omega+\oint_{\Gamma_{\sigma n}}T_0\cdot u\,ds\\&-\sum_j\Big[\int_{\Omega_n^*\cap\Omega_j}\sigma^T\Big(B\left(\frac{\partial}{\partial x_i}\right)u\Big)d\Omega-\oint_{\Gamma_{nj}}T\cdot u\,ds\Big]\Big\}\\&=\text{stationary},\end{aligned} \tag{2.4}$$

where σ = stresses,

u = displacements assumed to satisfy the prescribed boundary conditions,

$\{\Omega_n^*\}$ = a subdivision of Ω associated with the stresses,

$\{\Omega_j\}$ = another subdivision of Ω associated with the displacements, such that for any pair $(\Omega_j,\ \Omega_n^*)$ of subdomains $\partial(\Omega_j\cap\Omega_n^*)\backslash\partial\Omega_n^*$ either is empty or runs through the interior of Ω_n^*,

$\Gamma_{nj}=\partial(\Omega_n^*\cap\Omega_j)\backslash\partial\Omega_n^*$.

Contrasting this with the Hellinger-Reissner Principle, which can be expressed as

$$\begin{aligned}\Pi_R=-\sum_n\Big\{&\int_{\Omega_n^*}\Big[\frac{1}{2}\,\sigma^TD^{-1}\sigma+f\cdot u-\sigma^T\Big(B\left(\frac{\partial}{\partial x_i}\right)u\Big)\Big]d\Omega+\oint_{\Gamma_{\sigma n}}T_0\cdot u\,ds\Big\}\\&=\text{stationary},\end{aligned}$$

we see the following differences between the two variational principles:

1) The terms of surface integral $\sum_n \sum_j \oint_{\Gamma_{nj}} T \cdot u ds$ appear in the new principle;

2) The bilinear functional $\Pi_R(\sigma, u)$ is defined on $(L_2(\Omega))^6 \times (H^1_{u_0}(\Omega))$ where $H^1_{u_0}(\Omega) = \{u \in (H^1(\Omega))^3 : u|_{\Gamma_u} = u_0\}$ and $H^1(\Omega)$ = Sobolev space, whereas Π^*_R is defined on $H_V \times H_U(u_0)$, where

$$H_V = \left\{\sigma \in [L_2(\Omega)]^6 : B^T\left(\frac{\partial}{\partial x_i}\right)\sigma\Big|_{\Omega_n^*} \in [L_2(\Omega_n^*)]^3, \quad n=1, 2, \cdots\right\}$$

and $$H_U(u_0) = \{u \in [L_2(\Omega)]^3 : u|_{\Omega_j} \in [H^1(\Omega_j)]^3,\ j=1, 2, \cdots, u|_{\Gamma_u} = u_0\}.$$

In other words, the continuity of permissible displacements at the intersubdomain boundaries $\partial\Omega_j \backslash \partial\Omega$ is relaxed with the new principle at the expense of constrained stresses so that the surface tractions T are continuous almost everywhere at $\partial\Omega_j \backslash \partial\Omega$.

Fortunately the additional continuity requirement for T can be easily satisfied as for the finite element implement of the new principle since $\{\sigma \in [L_2(\Omega)]^6 : \sigma|_{\Omega_n^*} =$ polynomials, $n=1, 2, \cdots,\} \subset H_V$. Therefore such variational principle has actually been obtained in which both the permissible displacements and the permissible stresses are piecewise continuous.

Thus the mixed stiffness finite element method for approximating the problem (2.1)—(2.3) consists in seeking a saddle point (σ_h, u_h) of Π^*_R on finite element subspaces $V_h \times U_h \subset H_V \times H_U$. More specifically, on $V_h \times U_h$, we obtain its discrete problem:

Find $(\sigma_h, u_h) \in V_h \times U_h(u_0)$ such that

$$d(\sigma_h, \sigma) - E(\sigma, u_h) = 0, \ \forall \sigma \in V_h \tag{2.5}$$

$$E(\sigma_h, v) = \int_\Omega f \cdot v d\Omega + \oint_{\Gamma_\sigma} T_0 \cdot v ds, \ \forall v \in U_h(0), \tag{2.6}$$

where $$d(\sigma, \tau) = \sum_n \int_{\Omega_n^*} \sigma^T D^{-1} \tau d\Omega,$$

$$E(\sigma, v) = \sum_n \sum_j \left[\int_{\Omega_n^* \cap \Omega_j} \sigma\left(B\left(\frac{\partial}{\partial x_i}\right)u\right) d\Omega - \oint_{\Gamma_{nj}} T \cdot v ds\right]$$

$$= \sum_j \left(\int_{\Omega_j} \sigma\left(B\left(\frac{\partial}{\partial x_i}\right)u\right) d\Omega - \oint_{\partial\Omega_j \backslash \partial\Omega} T \cdot v ds\right],$$

$U_h(\varphi)$ = finite element subspace such that the boundary condition φ is satisfied at boundary nodes.

We find this method attractive in the following features:

(1) The degrees of freedom associated with stress variables can be eliminated at element level. Then, as will be seen in the next section, the pattern of the standard finite element process is not violated and the available resources of finite element computer programs can be shared by the mixed stiffness method.

(2) Any piecewise polynomials which are elected according only to both the requirement of accuracy and computational economy can be used as displacement functions. Then the losses of computational efficiency in the standard methods from making the displacements satisfy the compatible conditions can be averted.

Owing to this point, just as will be seen later, we succeed in improving the isoparametric elements of the serendipity family.

(3) In addition to the variational principle, the convergence of mixed stiffness

finite element solutions is assured mainly by choosing the appropriate stress functions. Since stresses need not obey any constraint, there is plenty of room for this choice.

For the details of mathematical foundations of the method and other applications, see [8—13].

3. Direct Formulation of 14-node Element Characteristics

3.1. Shape of element and coordinate transformation

The shape of 14-node mixed stiffness element is almost the same as the 20-node isoparametric element in a Cartesian Space. It is obtained as well by distorting a cube in the manner indicated in Fig. 1.

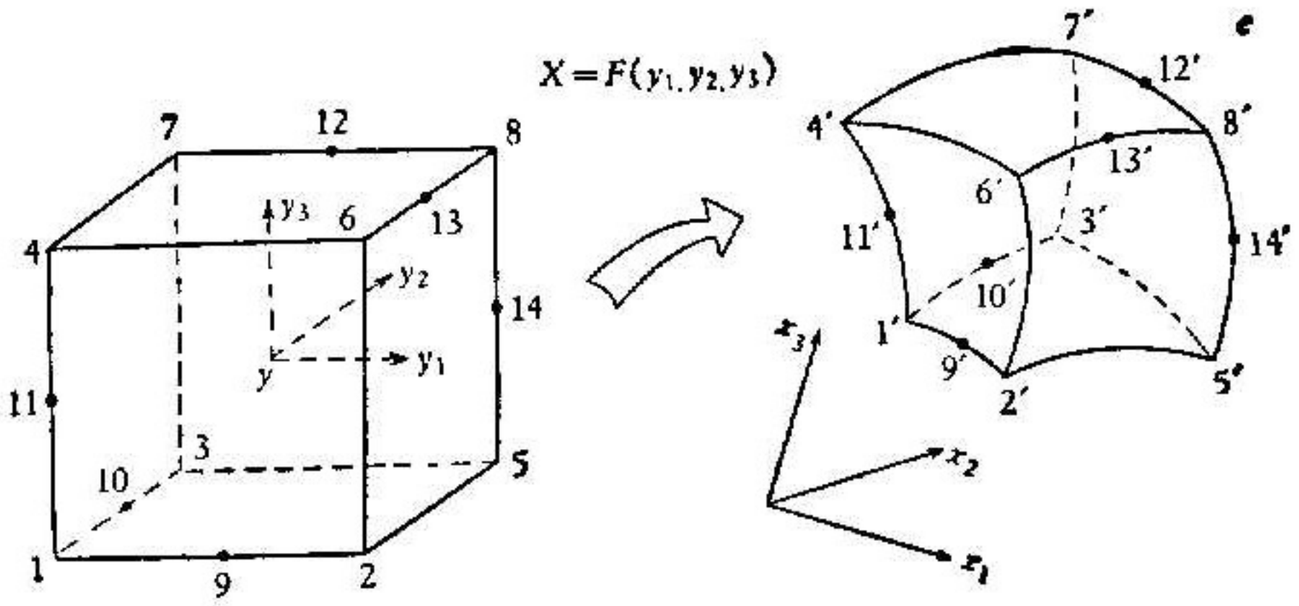

Fig. 1 Three dimensional "mapping" of a cubical element

In order to establish a certain one-to-one correspondence between Cartesian and curvilinear coordinates, a typical element e and its referential cube are first divided into equal number of flat or curved tetrahedra. The continuous one-to-one correspondence between every tetrahedron and its dual body can be established by piecewise quadric polynomials. Then we get

$$X=\begin{bmatrix} x_1 \\ x_2 \\ x_3 \end{bmatrix}=F(y_1,\ y_2,\ y_3)=[N'_1,\ N'_2,\ \cdots,\ N'_t]\,X_0, \tag{3.1}$$

where N'_i = piecewise polynomials of degree $\leqslant 2$. Apart from the curved "boundary" element, N'_i are piecewise linear in the remaining case.

X_0 = column vector of Cartesian coordinate of "shape nodes" describing the form of elements. The "shape nodes" consist generally of 8 corner nodes except that the curved boundary element needs a fresh supply of "mid-side" points.

Under Ciarlet and Raviart's regularity conditions (cf. [3], § 4.3), the mappings F are indeed one-to-one continuous and their Jacobians J_F do not vanish provided $h=\mathrm{diam}(e)$ is small enough.

3.2. Displacement function and stress function

Just as the isoparametric elements, it suffices to represent these functions explicitly on a referential cube.

For the mixed stiffness quadratic element, the displacement nodes consist of 8 corner points and 6 mid-side points as shown in Fig. 1. Such arrangement of nodes guarantees 6 nodes well on each flat face. It is not only necessary for determining uniquely the displacements represented by quadric polynomials on each flat face, but its making the total number of nodes more than 10 is also sufficient for these nodal parameters to be able to represent any completely quadric polynomial. Thus the permissible displacements at any point within a typical element e can be defined as a

column vector

$$u=\begin{Bmatrix} u_1 \\ u_2 \\ u_3 \end{Bmatrix}=\begin{Bmatrix} \tilde{N} & & \\ & \tilde{N} & \\ & & \tilde{N} \end{Bmatrix}\begin{bmatrix} q_u^{(1)} \\ q_u^{(2)} \\ q_u^{(3)} \end{bmatrix}_e=[N]\{q_u\}_e, \tag{3.2}$$

where $\{q_u\}_e$ denotes a list of nodal displacements for a particular element. $\tilde{N}$ are shape functions not in a normal but in a generalized sense. Since no quadric polynomial can simultaneously satisfy the fourteen conditions of Lagrangian interpolation, actually $\tilde{N}$ are piecewise polynomials but globally discontinuous functions. The cube is divided into two parts by the discontinuous surface Γ. In the part containing the node No. 1,

$$\tilde{N}=[N_1, N_2, N_3, \cdots, N_{13}, N_{14}],$$

where $N_8=N_{12}=N_{13}=N_{14}=0$,

$$N_1=2\xi_4\left(\xi_4-\frac{1}{2}\right)-3(\xi_2\xi_1+\xi_2\xi_3+\xi_1\xi_3),$$

$$N_2=\xi_1(2\xi_1-\xi_3-\xi_2-1),$$

$$N_3=\xi_2(2\xi_2-\xi_1-\xi_3-1),$$

$$N_4=\xi_3(2\xi_3-\xi_2-\xi_1-1),$$

$$N_5=\xi_2\xi_1, \qquad N_9=4\xi_1(1-\xi_1),$$

$$N_6=\xi_1\xi_3, \qquad N_{10}=4\xi_2(1-\xi_2),$$

$$N_7=\xi_2\xi_3, \qquad N_{11}=4\xi_3(1-\xi_3)$$

and $(\xi_1, \xi_2, \xi_3, \xi_4)$ are the volume coordinates defined by four nodes No. 2, 3, 4, 1. In the other part, $\tilde{N}$ are defined in a similar manner.

In addition, it is worth pointing out that the $\partial\Omega_i\backslash\partial\Omega$ in (2.4) consist of the images of the surface Γ through the bijections F.

The permissible stress σ can also be defined as a column vector

$$\sigma=[\Psi]\{q_\sigma\}_e \tag{3.3}$$

in which $\{q_\sigma\}_e$ denotes a listing of nodeless variables and the elements of matrix $[\Psi]$ are piecewise polynomials of degree 1 and must be continuous at Γ. This construction of $[\Psi]$ can reduce the calculation of the inverse matrix in (3.7) and ensure the convergence criterion 2 in Sect. 4.

3.3. Approximate stress-strain relationship

In the mixed stiffness method, the relationship between stress and strain is not derived from the generalized Hooke's law and the strains determined by the displacements with differential relation, but from the variational formulation (2.4). In fact, since $d(\sigma, \sigma)_e$ is of a positive definite form, for the displacement u, expressed in terms of given nodal displacement vector q_u by using the relation (3.2), there exists a unique stress $\sigma_u=[\Psi]q_\sigma(u)$ such that

$$d(\sigma_u, \sigma)_e=E(\sigma, u)_e, \ \forall\sigma\in V_h. \tag{3.4}$$

Let us define two matrices

$$\tilde{S}=\int_e [\Psi]^T D^{-1}[\Psi]d\Omega, \tag{3.5}$$

$$\tilde{B}=\sum_j\left\{\int_{e\cap\Omega_j}[\Psi]^T B\left(\frac{\partial}{\partial x_i}\right)[N]d\Omega-\oint_{\Gamma_{ej}}[T([\Psi])]^T[N]ds\right\}, \tag{3.6}$$

where $\Gamma_{ej}=\partial(e\cap\Omega_j)\backslash\partial e$ are the surfaces at which the displacements u are discon-

tinuous, $T([\Psi]) = B^T(\cos(n, x_i))[\Psi]$.

Then a matrix equation equivalent to (3.4) is as follows

$$\tilde{S}\mathbf{q}_\sigma(u) = \tilde{B}\mathbf{q}_u$$

or

$$\sigma_u = [\Psi]\mathbf{q}_\sigma(u) = [\Psi]\tilde{S}^{-1}\tilde{B}\mathbf{q}_u \tag{3.7}$$

which is the desired stress-strain relationship in a discrete form.

Remark. Since it is different from the assumed stress hybrid method that the permissible stresses do not obey any equilibrium constraints in the mixed stiffness method, the $\tilde{S}^{-1}$ in (3.7) does not imply more calculation of element stiffness matrix needs more computer time than that of the conventional isoparametric element, even if it is able to evaluate the inverse matrix $\tilde{S}^{-1}$ economically by using a few inverse matrices of lower order.

3.4. Equivalent nodal forces and element stiffness matrix

Let linear operator T_h: $U_h \to V_h$ be the displacement-stress relationship defined piecewise by equations (3.4). The finite element variational problem (2.5), (2.6) can be reduced to: Find $u_h \in U_h(u_0)$ such that

$$\sum_e E(T_h u_h, v)_e = \int_\Omega f \cdot v \, d\Omega + \oint_{\Gamma_\sigma} T_0 \cdot v \, ds, \quad \forall v \in U_h(0). \tag{3.8}$$

Physically, this is a virtual work principle in a discrete form. Following the typical steps of the conventional finite element procedure (see [14], ch. 2), the nodal forces $\{F\}_e$ equivalent statically to the boundary stresses and distributed loads on the element are written as

$$\{F\}_e = \tilde{B}^T\tilde{S}^{-1}\tilde{B}\mathbf{q}_u + \{F_f\}_e + \{F_t\}_e, \tag{3.9}$$

where $[K] = \tilde{B}^T\tilde{S}^{-1}\tilde{B}$ is the stiffness matrix,

$\{F_f\}_e = -\int_e [N]^T \cdot f \, d\Omega$ are nodal forces due to distributed loads,

$\{F_t\}_e = -\oint_{\Gamma_\sigma \cap \partial e} [N]^T \cdot T_0 \, ds$ are nodal forces due to boundary stresses.

Once the nodal displacements $\mathbf{q}_u^h$ have been determined by solution of the overall "structural" type equations, the stresses at any point of the element can be found from the weighted averages over the relation (3.7) and the following

$$\sigma^h = DB\left(\frac{\partial}{\partial x_i}\right)[N]\mathbf{q}_u^h \tag{3.10}$$

Theoretically, the relations (3.7) and (3.10) are equally efficient. But calculations in Sect. 5 demonstrates that (3.7) is more accurate.

We conclude this section with the remark that the linear element with 8 nodes and the cubic element with 26 nodes in the family can be obtained respectively by constraining the nodal displacements at mid-side points and adding one node at every edge. Of course, the permissible stress functions should also change and the piecewise polynomials of degree 0 and 2 can be used correspondingly.

4. Convergence Analysis

In view of the complex form of nonstandard finite element methods, such as assumed stress hybrid model and mixed stiffness model, it seems very difficult to

ensure the convergence to the correct result, as known from the discussion on preventing any kinematic deformation models in [7]. Considerable efforts have been made in the last ten years to give a complete mathematical analysis of non-standard finite element methods[2-6,8-10]. As far as the mixed stiffness method is concerned, three convergence criteria (which can be considered as an extension of the three criteria for the conventional finite element methods) are available.

1) Consistency criterion. The displacement and stress functions should be so chosen that the following equalities hold almost everywhere at interfaces between subdomains of both the displacement and stress partitions:

$$B(\cos(n, x_i))(\sigma_+ - \sigma_-)\cdot(u_+ - u_-) = 0, \tag{4.1}$$

where $\sigma_+ - \sigma_-$ (or $u_+ - u_-$) = the jump of function σ (or u) at interfaces,
n = the unit outward normal to the interfaces.

In [9, 8], this is term the condition of virtual work for the jumps and it is pointed out that the condition ensures the consistency of finite element schemes with the approximated problems.

In the case of $V_h = DB\left(\frac{\partial}{\partial x_i}\right) U_h$, i. e. of conventional displacement approach, this is equal to the continuity criterion since condition (4.1) will not hold unless the displacement functions are continuous.

2) Zero energy mode criterion. The chosen displacement and stress functions should be such that the zero work condition:

$$E(\sigma, u)_{(e)} = \sum_j \left[\int_{e\cap\Omega_j} \sigma^T B\left(\frac{\partial}{\partial x_i}\right) u \, d\Omega - \oint_{\Gamma_{ej}} T\cdot u \, ds\right] = 0, \quad \forall \sigma \in V_h \tag{4.2}$$

holds only if the nodal displacements are caused by a rigid body displacement.

Mathematically, it has to ensure that condition (4.2) implies

$$\sum_j \left[\int_{e\cap\Omega_j} \left| B\left(\frac{\partial}{\partial x_i}\right) u\right|^2 d\Omega + \oint_{\Gamma_{ej}} |u_+ - u_-|^2 ds\right] = 0.$$

It has been proved[8,10] that this condition is sufficient and necessary for the Babuska-Brezzi inequality to be satisfied. Therefore the condition is crucial for the existence and convergence of mixed stiffness finite element solutions, as known from [2, 8, 10].

3) Constant stress criterion. The displacement and stress functions have to be of such a form that if nodal displacements and node stress parameters are compatible with a constant strain-stress condition, such constant strain and constant stress will in fact be obtained.

Provided that the requirements of Criterian 1 and 2 are satisfied, by one of the main results in [2, 8, 10], we have the following error estimate

$$\|\tilde{\sigma} - \sigma_h\|_V + \|\tilde{u} - u_h\|_U \leqslant C\{\inf_{u\in U_h(u_0)} \|\tilde{u} - u\|_U + \inf_{\sigma\in V_h} \|\tilde{\sigma} - \sigma\|_V\},$$

where $\|\sigma\|_V^2 = \|\sigma\|_{0,\Omega}^2 + \sum_i h_i^2 \|\sigma\|_{1,\Omega_i}^2$,

$$\|u\|_U^2 = \sum_j \left[\left\| B\left(\frac{\partial}{\partial x_i}\right) u\right\|_{0,\Omega_j}^2 + h_j^{-1} \oint_{\partial\Omega_j} |u_+ - u_-|^2 \, ds\right].$$

Then it is obvious from the interpolation theory in the Sobolev spaces[3] that the constant stress-strain condition implies $\|\tilde{\sigma} - \sigma_h\|_V + \|\tilde{u} - u_h\|_U = O(h)$ $(h = \max h_j)$, i. e. the convergence of mixed stiffness finite element solution (σ_h, u_h) to an exact solution

$(\tilde{\sigma}, \tilde{u})$ with the decreasing element size h.

It can be verified that the 14-node mixed stiffness element satisfies all of the three criteria at least in the case that h is small enough, but we do not intend to discuss it here and skip the detailed mathematical analysis, especially the error estimates of $\|\tilde{\sigma}-\sigma_h\|_V+\|\tilde{u}-u_h\|_U=O(h^2)$ and $\|\tilde{u}-u_h\|_{0,\Omega}=O(h^3)$, to the forthcoming paper.

5. Numerical Experiments

In order to test the computational efficiency of the 14-node mixed stiffness element and to make a few observations, we will check some numerical results and compare them with the results of the 20-node isoparametric element. All the computations were performed on a Siemens 7760 computer in double precision arithmetic, by using SAP-5 and MISEP programs, for the calculations concerned with isoparametric elements of the serendipity family and 14 nodes mixed stiffness element respectively. The MISEP program is obtained by inserting the new element stiffness generation and other subroutines into SAP program written in [1].

Example 1. We consider the finite element stress analysis of an elastic prism with curved boundary which is subjected to distributed loads

$$f=\begin{bmatrix} f_1 \\ f_2 \\ f_3 \end{bmatrix}=-\frac{E(1-\nu)}{(1+\nu)(1-2\nu)}\begin{bmatrix} (x_1+1)\left[\ln(x_1+1)+\frac{5}{6}\right] \\ (x_2+1)\left[\ln(x_2+1)+\frac{5}{6}\right] \\ (x_3+1)\left[\ln(x_3+1)+\frac{5}{6}\right] \end{bmatrix}$$

in which $E=7.2\times10^5$, $\nu=0.23$ and kinematic boundary conditions $u_0=u|_{\partial\Omega}$ where u is the exact displacement solution

$$u=\begin{bmatrix} u_1 \\ u_2 \\ u_3 \end{bmatrix}=\frac{1}{6}\begin{bmatrix} (x_1+1)^3\ln(x_1+1)+6x_2x_3 \\ (x_2+1)^3\ln(x_2+1)+6x_1x_3 \\ (x_3+1)^3\ln(x_3+1)+6x_1x_2 \end{bmatrix}.$$

The domain Ω occupied by the prism is as follows

$$\Omega=\left\{(x_1,\ x_2,\ x_3):\ \begin{array}{l} -1\leqslant x_1\leqslant y_1(x_2) \\ -1\leqslant x_2\leqslant y_2(x_1) \\ -1\leqslant x_3\leqslant 1 \end{array}\right\},$$

where $y_1=1+0.1\sin\pi x_2$, $y_2(x_1)=1-0.1\sin\pi x_1$. The cross section Ω_0 of Ω and its 6×6 grid are shown in Fig. 2.

By dividing Ω into $n\times n\times n$ prism element ($n=2$, 4, 5, 6), the finite element stress analysis was carried out by employing the 14-node mixed stiffness element and 20-node isoparametric element respectively. The averaged relative errors between the exact and approximate nodal displacements (resp. stresses), expended CPU time and some referential data such as total number of nodes, bandwidth and so on, are presented in Table 1. The calculations by different elements are denoted respectively by the symbol strings MIS14 and ISO20 in the Table 1.

Table

N_e=Number of elements
N_t=Total number of nodes
N_h=Number of equations
W_b=Maximum bandwidth
W_m=Mean half bandwidth

Examples		Elements	Items: Referential data					Items: Computer time (cpu:sec)				
			N_e	N_t	N_h	W_b	W_m	T_i	T_c	T_e	T_s	T_t
			Results									
2×2×2 Subdivision	Ex. 1	ISO20	8	81	243	123		1	36	3.125	30	67
		MIS14	8	57	21	18	10	1	13	1.3	2	16
	Ex. 2	ISO20	8	81	243	123		1	38	3.25	32	71
		MIS14	8	57	21	18	10	1	13	1.3	2	16
4×4×4 Subdivision	Ex. 1	ISO20	64	425	1275	321		4	309	2.9	870	1183
		MIS14	64	281	261	108	70	6	101	1.3	28	135
		ISO14	64	281	843	216		3	167	1.77	280	451
	Ex. 2.	ISO20	64	425	1275	321		4	366	2.97	998	1368
		MIS14	64	281	261	108	70	6	104	1.3	27	137
		ISO14	64	281	843	216		3	191	1.81	305	499
5×5×5 Subdivision	Ex. 1	ISO20	125	756	2268	456		7	683	2.79	3189	3879
		MIS14	125	486	552	174	120	9	198	1.3	102	309
		ISO14	125	486	1458	303		4	413	1.77	1059	1476
	Ex. 2	ISO20	125	756	2268	456		6	678	2.78	3160	3845
		MIS14	125	486	552	174	120	10	201	1.3	102	313
		ISO14	125	486	1458	303		4	420	1.81	1070	1494
6×6×6 Subdivision	Ex. 1	ISO14	216	793	2379	405		7	650	1.67	2631	3283
		MIS14	216	793	1077	249	187	15	338	1.3	383	736
	Ex. 2	ISO14	216	793	2379	405		7	667	1.69	2625	3299
		MIS14	216	793	1077	249	187	15	348	1.3	380	743
2×1×8 (beam)	Ex. 3	ISO20	16	165	470	119		1	83	4.31	32	118
		MIS14	16	100	305	63	42	1	24	1.3	9	34
		ISO14	16	110	305	63		1	31	1.56	15	47

1

T_i=Time for input phase
T_c=Time for calculation of structure stiffness matrix and total load vector
T_e=Time for calculation of element stiffness matrix
T_s=Time for static analysis
T_t=Total solution time

Averaged relative errors						
Displacements: $\sum_{i=1}^{NA} \frac{\lvert u(p_i)-u_h(p_i)\rvert}{N_h \max_i \lvert u(p_i)\rvert}$	Stresses: $\sum_{i}^{m} \frac{\lvert\sigma(Q_i)-\sigma_h(Q_i)\rvert}{m \max_i \lvert\sigma(Q_i)\rvert} \triangleq \Delta(\sigma)$					
	$\Delta(\sigma_{x_1x_1})$	$\Delta(\sigma_{x_2x_2})$	$\Delta(\sigma_{x_3x_3})$	$\Delta(\sigma_{x_1x_2})$	$\Delta(\sigma_{x_2x_3})$	$\Delta(\sigma_{x_3x_1})$
0.055284	0.105946	0.121936	0.068596	0.277989	0.026991	0.043778
0.004079	0.019460	0.020216	0.016532	0.026286	0.051769	0.053660
0.573966	0.527705	0.210669	0.247688	0.776681	0.125374	0.132401
0.060946	0.261033	0.108978	0.128128	0.364076	0.128826	0.310248
0.001668	0.015904	0.016433	0.016173	0.009935	0.003955	0.005120
0.001667	0.004692	0.004446	0.005370	0.008760	0.015351	0.013205
0.005924	0.075916	0.075782	0.076258	0.033644	0.028044	0.026860
0.090049	0.097215	0.077177	0.047921	0.139455	0.173906	0.075996
0.023859	0.081863	0.040221	0.040592	0.069853	0.041249	0.062537
0.095916	0.297453	0.159784	0.179051	0.186285	0.168450	0.118084
0.001001	0.010174	0.010431	0.010298	0.005837	0.002285	0.002709
0.000957	0.003627	0.004617	0.003561	0.009648	0.009375	0.008268
0.003739	0.059874	0.059327	0.059438	0.031616	0.026434	0.023146
0.073298	0.056244	0.076522	0.033529	0.119814	0.161749	0.045619
0.014720	0.047082	0.022788	0.025025	0.048518	0.026795	0.046026
0.079842	0.238566	0.149771	0.142615	0.163284	0.175408	0.094392
0.002074	0.051688	0.050761	0.051017	0.029232	0.024949	0.022008
0.000695	0.002871	0.004036	0.002729	0.007799	0.007195	0.006223
0.055408	0.207548	0.140943	0.125184	0.155378	0.169944	0.087218
0.008751	0.032695	0.015804	0.017122	0.033246	0.017458	0.030863
Maximum displacement (-6.912×10^{-4})	-7.0183×10^{-4}		Maximum stress (-432)		-444.8	
	-6.9984×10^{-4}				-391.6	
	-5.3827×10^{-4}				-410.7	

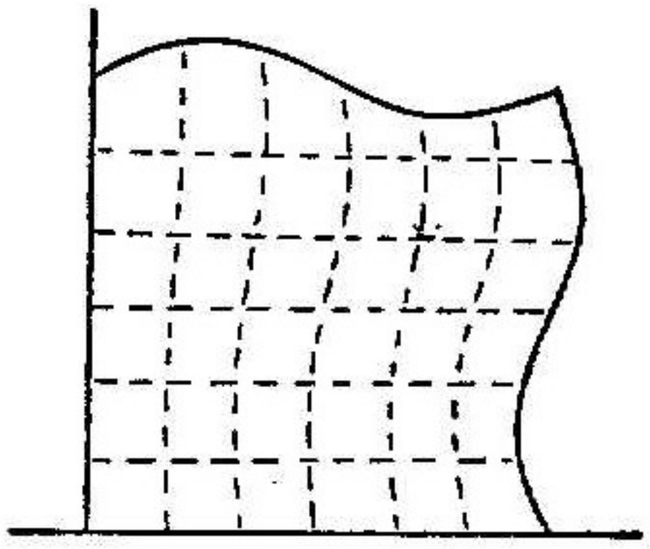

Fig. 2 The cross section of the prism and 6×6 grid

In order to make another comparison, the third kind of calculations was carried out by 14–node isoparametric element on every grid, which is achieved by constraining linearly 6 nodal parameters of the 20–node element so that the arrangement of its nodes is the same as the 14–node mixed stiffness element. In Table 1, this kind of calculation is denoted by symbol string ISO14. Although the numbers of the nodes on two sorts of elements are equal, the degrees of accuracy shown in Table 1 form a sharp contrast. The numerical results confirm the theoretical conclusion that the 14–node isoparametric element is only linear but the 14–node mixed stiffness element is quadric.

Example 2. Except the distributed loads and kinematic boundary conditions, Examples 2 and 1 are the same in all other aspects. In Example 2, we consider such loads and boundary conditions that the boundary value problem (2.1)—(2.3) has a unique solution of the following form:

$$u=\begin{bmatrix} u_1 \\ u_2 \\ u_3 \end{bmatrix}=\begin{bmatrix} \sin 3(x_2x_3+x_1) \\ \sin(x_3x_1+x_2) \\ \cos 2(x_1x_2+x_3) \end{bmatrix}.$$

Hence the distributed loads considered in the calculations are as follows:

$$f=\begin{bmatrix} f_1 \\ f_2 \\ f_3 \end{bmatrix}=\frac{E}{(1+\nu)(1-2\nu)}$$

$$\times\begin{bmatrix} 9\sin 3(x_2x_3+x_1)\left[(1-\nu)+\frac{1-2\nu}{2}(x_2^2+x_3^2)\right]+\frac{1}{2}[x_3\sin(x_1x_3+x_2) \\ \quad +4x_2\cos(x_1x_2+x_3)] \\ \sin(x_1x_3+x_2)\left[(1-\nu)+\frac{1-2\nu}{2}(x_1^2+x_3^2)\right]+\frac{1}{2}[9x_3\sin(x_2x_3+1) \\ \quad +4x_1\cos 2(x_1x_2+x_3)] \\ 4\cos 2(x_1x_2+x_3)\left[(1-\nu)+\frac{1-2\nu}{2}(x_1^2+x_2^2)\right]+\frac{1}{2}[9x_2\sin(x_2x_3+x_1) \\ \quad +x_1\sin(x_1x_3+x_2)] \end{bmatrix}.$$

For numerical results, see Table 1.

Example 3. Consider the 3–dimensional finite element stress analysis of a simply-supported beam (Fig. 3).

In the case, the exact solution of the problem is unknown. Then in Table 1, the maximum deflection 0.6912×10^{-4} and the maximum stress 432 on the symmetrio

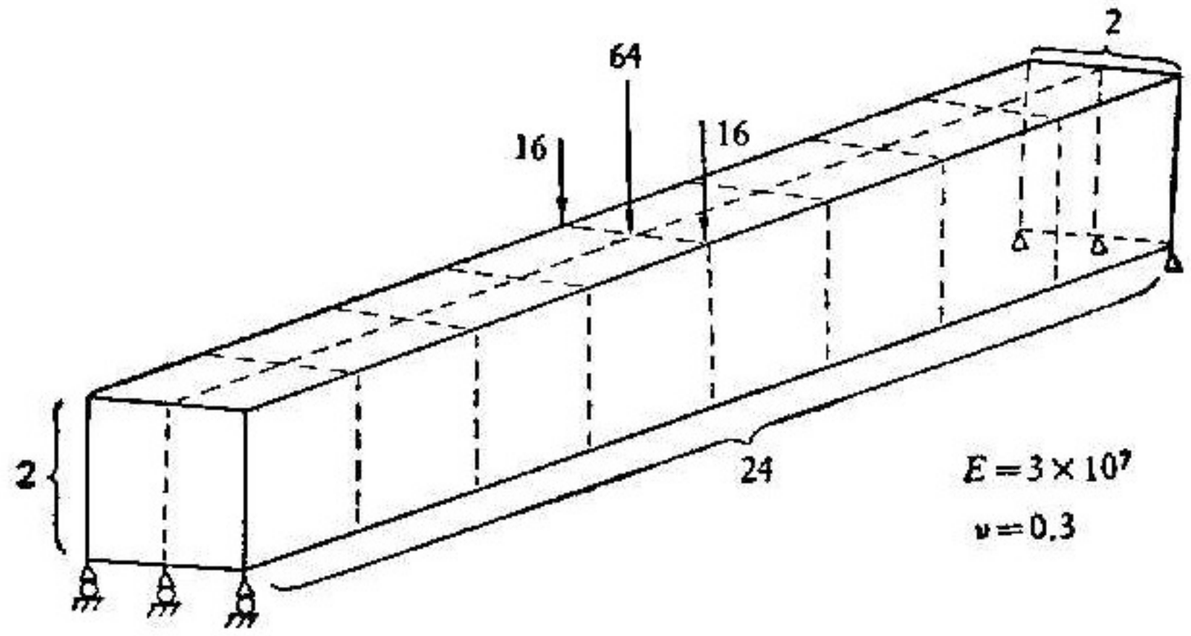

Fig. 3 The simply-supported beam subjected to concentrated loads

middle face obtained from classical beam theory are used as a referential standard of accuracy for the comparison between the various numerical results obtained by the different elements.

Example 4. In addition to 3-dimensional stress analysis, we also consider the problem

$$-\Delta u=(1-x_1^2)(1-x_2^2)+(1-x_2^2)(1-x_3^2)+(1-x_3^2)(1-x_1^2)$$
$$\text{in } \Omega=(0,1)\times(0,1)\times(0,1),$$
$$u|_{\partial\Omega}=0,$$

where the exact solution $u=\frac{1}{2}(1-x_1^2)(1-x_2^2)(1-x_3^2)$.

The numerical results obtained by using 14-node mixed stiffness element are shown in Table 2(see[9], too):

Table 2

$\ln h$	Regular mesh	Irregular mesh(any four vertices of an element might be noncoplanar)
	$\ln\left(\sum_{i=1}^{N_h}\frac{\lvert u(p_i)-u_h(p_i)\rvert}{N_h}\right)$	$\ln\left(\sum_{i=1}^{N_h}\frac{\lvert u(p_i)-u_h(p_i)\rvert^2}{N_h}\right)^{\frac{1}{2}}$
−0.69314	−5.2155	−4.9764
−0.91629	−5.8608	−5.7264
−1.38629	−7.4770	−7.4279

They imply that

$$\ln\left[\sum_{i=1}^{N_h}|u(p_i)-u_h(p_i)|^2\Big/N_h\right]^{\frac{1}{2}}\leqslant 3\ln h+\text{const.}$$

Hence $$\|\Pi u-u_h\|_{0,\Omega}\leqslant C_f\left(\sum_{j=1}^{N_h}|u(p_i)-u_h(p_i)|^2\right)^{\frac{1}{2}}\leqslant C_f h^3,$$

where $\Pi: H^3(\Omega)\cap H_0^1(\Omega)\to U_h$ is a Lagrangian interpolator. Then Table 2 shows that $\|u-u_h\|_{0,\Omega}\leqslant\|u-\Pi u\|_{0,\Omega}+\|\Pi u-u_h\|_{0,\Omega}=O(h^3)$, i. e. optimal rate of convergence occurs as well.

In addition, we found through the numerical observations that there exist stress "good" points at which more accurate approximate stresses can be obtained.

6. Conclusion

To sum up, the 14–node mixed stiffness element is superior over the 20–node isoparametric element because of the following reasons:

1) The mixed stiffness element and isoparametric element are equally satisfactory in the data preparation, the flexibility for ccmplex geometry and the same rate of convergence. Furthermore, as shown in Table 1, an improvement of accuracy arises with the same meshes when the new element is used.

2) The computing time needed to evaluate the stiffness matrix of the new element is one half less than that for the isoparametric element when $3\times3\times3$ Gauss integration rule is used.

3) Since the total number of nodes and the mean half bandwidth of new and old elements is of a ratio of about $5n+3$ to $8n+2$(i. e. $(n+1)^2\frac{(5n+3)}{2}:\ (n+1)^2(4n+1)$) for $n\times n\times n$ subdivision, the amount of data needed to store in the two methods is of a ratio of about one to two, and the computational efficiency of the 14–node mixed stiffness element is 3—4 times the 20–node isoparametric element because the number of arithmetical operations for the triangulation of the sparse matrix is roughly equal to const. $\times$ (total number of nodes) $\times$ (mean half bandwidth)^2 and hence the computing time(CPU) for the triangulation in the two methods is of a ratio of about $(5n+3)^3$ to $(8n+2)^3$.

The substantial improvement of computational efficiency has been in fact confirmed by the total solution times corresponding to ISO20 and ISO14 in Table 1.

References

[1] K. J. Bathe, E. L. Wilson, Numerical Methods in Finite Element Analysis, Prentice-Hall, Inc., Englewood Cliffs, N. J., 1976.

[2] F. Brezzi, *RAIRO ser. Numer. Anal.*, 8(1974), 129—151.

[3] P. G. Ciarlet, The Finite Element Method for Elliptic Problems, North-Holland, 1978.

[4] R. S. Falk, J. E. Osborn, *RAIRO ser. Numer. Anal.*, 14(1980), 249—277.

[5] R. Glowinski, E. Y. Rodin, O. C. Zienkiewicz, edited, Energy Methods in Finite Element Analysis, John Wiley & Sons, 1979.

[6] C. Johnson, B. Mercier, *Numer. Math.*, 30(1978), 103—116.

[7] Theordore H. H. Pian, On Hybrid and Mixed Finite Element Methods, Presented at the Finite Element Invitational Symposium, May 19—23, 1981, Hefei, China.

[8] Zhou Tian-xiao, An Analysis of Mixed Stiffness Finite Element Method, *Acta Aeronautical Astronautica sinica*, 1978, 44—59.

[9] Zhou Tian-xiao, Mixed Stiffness Model and Unified Approach to Dual Saddle-Point Finite Element Analysis, Presented at the Finite Element Invitational Symposium, May 19—23, 1981, Hefei, China. (to appear)

[10] Zhou Tian-xiao, Equivalence Theorem for Saddle Point Finite Element Schemes and Two Criteria of Strong Babuska-Brezzi Condition, *Scientia Sinica*, 24(1981), 1190—1206.

[11] Zhou Tian-xiao, An Improvement on Mercier's Mixed Finite Element Model for the First Biharmonic Problem, *Mathematica Numerica Sinica*, 4(1982), 283—289. (in Chinese)

[12] Zhou Tian-xiao, A Mixed Stiffness Finite Element Method for the Navier-Stokes Equations(1), Presented at the China-France Symposium on Finite Element Methods, April, 19—23, 1982, Beijing, China. (to appear)

[13] Zhou Tian-xiao, *Mathematica Numerica Sinica*, 2(1980), 50—62. (in Chinese)

[14] O. C. Zienkiewicz, The Finite Element Method in Engineering Science, McGraw-Hill, 1971.